W-band Waveguide Antenna Elements for Wideband and Wide-Scan Array Antenna Applications For Beyond 5G

W-band Waveguide Antenna Elements for Wideband and Wide-Scan Array Antenna Applications For Beyond 5G

Yingqi Zhang, Artem R. Vilenskiy, Marianna V. Ivashina
Antenna Group, Dept. of Electrical Engineering, Chalmers University of Technology, 41296 Gothenburg, Sweden,
artem.vilenskiy@chalmers.se, yingqi@chalmers.se, marianna.ivashina@chalmers.se

***Abstract*—Energy-efficient and highly-compact beam-steering array antennas at W- and D-band frequencies are considered as future enabling technologies for beyond-5G applications. However, most existing solutions at these frequencies are limited to the fixed-beam and frequency-dependent beam-steering scenarios. This paper aims to fill in this knowledge gap by investigating various types of antenna elements as potential candidates for wideband and wide-scan arrays at W-band. We consider open-ended ridge and ridge gap waveguide radiating elements that could overcome the physical complexities associated with the integration of elements in large-scale electronically scanned arrays. An infinite array approach is used, where we have adopted a triangular array grid and introduced E- and H-plane grooves to the element design to enhance the scan and bandwidth performance. Cross-comparison of several simulated array designs leads to the final array elements with 25% impedance bandwidth over the scan range of $\pm 40^\circ$ in both the E- and H-planes.**

***Index Terms*—phased array antennas, beam steering, W-band, waveguide antenna element, ridge gap waveguide.**

I. Introduction

The development of future beyond-5G (B5G) wireless communication applications, products, and services strongly relay on innovative antenna technologies that can operate at higher bands of the mm-wave frequency spectrum (i.e. 100+GHz). The W-band (75–110 GHz) and D-band (110–170 GHz) are considered among most promising directions of development owing to the wide available bandwidth and relatively low atmospheric absorption loss, and have already been employed in the automotive radar applications as well as in backhauling and multi-user wireless communications.

Antenna systems for these future applications are required to have a much higher effective radiated power, as compared to the presently deployed 5G systems, in order to compensate for the increased material losses and reduced power generation ability of active electronic devices at higher frequencies. Other challenges include significantly smaller antenna dimensions, and, hence, tighter manufacturing tolerances and extra difficulties of integrating active integrated circuits (IC) (that become comparable in size with antenna elements) and signal routing, especially in large-scale arrays.

Due to the above-mentioned physical and manufacturing challenges, to date, most reported designs of high-gain, high-efficiency W-/D-band array antennas are for fixed-beam applications (often referred to as fixed wireless access). One example of such antenna technologies is LTCC on-package array antennas that have obvious integration advantages, but suffer from poor efficiency (typically, $< 35\%$) [1]. In contrast, hollow waveguide (WG) type antennas have much higher efficiency ($> 50\%$) [2], while benefiting from high-precision CNC-milling manufacturing techniques, but are less versatile in terms of beamforming capabilities as these require dedicated WG-to-IC transitions which are typically lossy and occupy much space. Recent developments in silicon micro-machining have demonstrated even higher efficiencies ($>70\%$) [3] thanks to their nanometer surface roughness. However, these are still at the research development stage. It is worth mentioning that there are available published beam-steering solutions for large-scale array antennas at W-/D-bands and higher frequencies, but these are limited to traveling-wave antennas with frequency dependent beam steering [4], [5], which are not practical for our targeted applications. Other 2D beam-steering solutions that are based on AoC (Antenna-On-Chip) and SiP (System-In-Package) implementations, as realized today at 60 GHz bands [6], have limited potential to simultaneously achieve the required wideband and wide-angle beam-steering performance with high radiation efficiency.

In the present work, we investigate and cross-compare various types of antenna elements as potential candidates for wideband and wide-scan 2D electronically scanned arrays at W/D-band. The considered designs include open-ended ridge waveguide and ridge gap waveguide radiating elements (this choice is motivated by the expected high efficiency), where we have introduced several modifications with respect to standard implementations in the form of E- and H-plane grooves. Furthermore, a triangular uniform array grid is chosen to enhance the grating lobe-free scan and bandwidth performance of the arrays of such antenna elements. The antenna array element is optimized to achieve the best bandwidth vs. scan range trade-off, subject to practical implementation constraints in terms of the size and complexities of the element geometrical features as well as the spacing needed to accommodate WG-to-IC transitions [7].

The structure of the paper is the following: Section II presents the designs of the considered array antenna elements

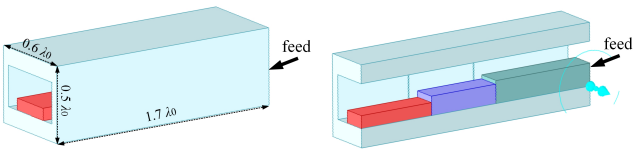

(a) Initial configuration of the open-ended ridge WG array element.

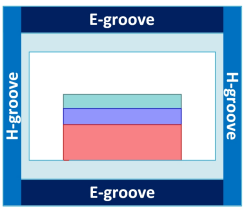

(b) Front view of the ridge WG element aperture with optional E- and H-plane grooves.

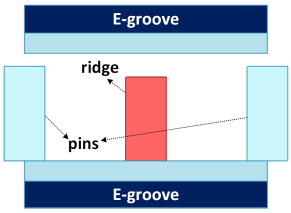

(c) Front view of the ridge gap WG (RGW) element aperture with optional E-plane grooves.

Fig. 1. Various types of array antenna elements

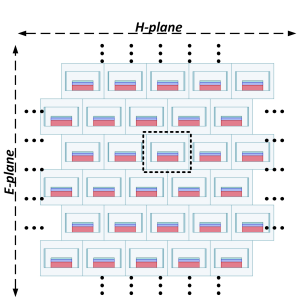

(a) Array grid

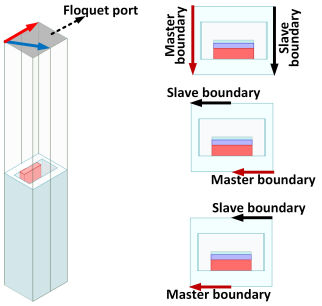

(b) Floquet port and boundary conditions

Fig. 2. Infinite array model

in the infinite array setup; Section III illustrates the simulated results of different array antenna elements; Section IV analyzes the results of design optimization and trade-off studies between the impedance bandwidth and beam-steering range. Finally, key observations and future directions of this work are summarized in Section V.

II. Array Antenna Element Designs

We consider the open-ended WG antenna element as the starting point of the array antenna design in this work, where such elements can be cascaded with active electronics to form independent beam-steering channels [8]. In this section, a set of open-ended WG elements are designed for the operation in the infinite array scenario.

A. Open-ended ridge waveguide antenna element

The initial design of the open-ended WG antenna array element is shown in Fig.1(a). A single ridge is adopted inside the WG structure to lower the cut-off frequency of its fundamental mode, thus providing a wideband low-dispersive operation [9] with transverse element size close to $0.5\lambda_0$ (λ_0 is the free-space wavelength corresponding to the central design frequency f_0). Various open-ended ridge WG elements have been studied previously including dual- and quad-ridge element designs [10], [11]. However, the reported wideband beam-steering performance was limited due to impedance mismatch (e.g., VSWR < 4 in the 11% bandwidth and 60° scan range for the X-band array element with half-wavelength E-plane size at central frequency in [10]). In this study, we employ several wideband techniques to improve the element's active reflection coefficient during beam steering.

The WG elements are arranged in a triangular array grid [see Fig. 2(a)] that has been chosen to relax the requirements on the array inter-element spacing in the H-plane [12]. This allows for $> 0.5\lambda_0$ inter-element-spacing for grating lobe-free wide-angle beam steering. The increased H-plane spacing is also beneficial for lowering the WG cut-off frequency and increasing the available physical space for active electronics integration behind the array aperture. As Fig. 2(a) shows, the inter-element spacing values were chosen as $0.5\lambda_0$ and $0.6\lambda_0$ in the E- and H-plane, respectively.

It is well know that open-ended WG array antennas have relatively strong antenna element mutual coupling effects [12], [10]. This can be a limiting factor of the bandwidth and scan range, where the latter often results in scan-blindness. This problem can be successfully overcome by adding grooves between the radiating WG elements [13]. These grooves operate as a soft surface, and hence, stop the electromagnetic waves propagation above the array aperture, thus effectively decoupling the array elements. To study this approach, we consider two additional ridge WG array elements: the element with only E-plane grooves, and the element with E- and H-plane grooves [Fig.1(b)]. In all cases, the two-step transformer is used to improve a wideband impedance matching with the free space: the ridge height is reduced in a stepped manner while the WG widens accordingly in the H-plane [see Fig. 1(a)].

B. Open-ended ridge gap waveguide (RGW) antenna element

The ridge WG element requires good electrical contacts between its sidewalls and is very sensitive to manufacturing errors and assembling misalignment. Such closed WG structures create additional implementation challenges when attempting the integration with active electronics and control lines tracing [8]. To address these problems, we propose a novel array element design based on an open-ended ridge gap waveguide (RGW) [14]. Its front view is shown in Fig. 1(c). The main advantage of the RGW design is its intrinsically contactless structure, which thereby allows for low-cost manufacturing, especially at high millimeter wave frequencies [14]. Also, the gap provides the desired extra space for ICs and WG-IC transition structures. The RGW unit cell sizes are the same as for the ridge WG element. We will consider two RGW element configurations: the initial design and the design loaded with E-plane grooves. The ridge height is again reduced at the aperture area to improve the impedance matching.

III. Simulation Results

To characterize the array antenna element beam-steering performance in large finite array configurations, we have employed a full-wave simulation model of the array unit cell. This unit cell model has sidewall periodic boundary conditions and Floquet port above the element aperture. The analysis was performed in the Ansys HFSS environment with the simulation setup as shown in Fig.2(b). The central design frequency is $f_0 = 95$ GHz. All the considered element designs have been optimized to maximize the impedance matching bandwidth for the broadside radiation. The magnitude of the active reflection coefficient ($|\Gamma|$) for the beam steering in the E- and H-planes is shown in Fig. 3.

First, the results for the initial ridge WG element configuration are presented [Fig.3(a)]. The black dashed line indicates the grating lobe-free border in the E-plane, where no grating lobes can exist in the H-plane inside the studied frequency-scan angle range. As seen, the impedance matching degrades when both the scanning angle and bandwidth increase. The exemplified targeted impedance bandwidth (BW) goals of 10% and 20% ($|\Gamma| \leq -10$ dB) are depicted by the pairs of dash-dotted lines. In the E-plane, the maximum scan angle (θ_{max}) reaches 56° for the 10% BW and 37° for the 20% BW at higher BW edge. However, $|\Gamma| > -10$ dB at lower frequencies (shaded area), hence the BW is always less than 20%. At the same time, in the H-plane, the 10% and 20% bandwidth goals are achieved at the higher BW edge for beam steering up to 25°, and 17°, respectively; on the other hand, the required matching at the lower BW edge can only be achieved for frequencies above 87 GHz. The scan-blindness can be observed nearby the grating lobe entering the visible region in the E-plane (upper right area of the plot).

The beam-steering performance of the ridge WG element with only E-plane grooves and with both E- and H-plane grooves is demonstrated in Fig. 3(b) and Fig. 3(c), respectively. The width and depth values of the grooves were optimized to improve the active reflection coefficient. When the E-plane grooves are added, the array demonstrates a significantly larger bandwidth for the broadside beam in both E- and H-planes. In the E-plane, θ_{max} reaches 47° and 37° for the 10% and 20% BW goals, respectively [Fig.3(b)]. In the H-plane, θ_{max} has been increased to 29° and 28° within the 10% and 20% BW, respectively. The E-plane scan-blindness has been fully mitigated. On the other hand, we can observe the appearing scan-blindness phenomena in the H-plane (upper right area of the plot) that is associated with the mutual coupling effects in the triangular grid as caused by the E-plane grooves.

Next, we analyze the results of the array antenna element design with E- and H-pane grooves. As observed in Fig.3(c), the beam-steering performances has been improved further, as compared to the above-described configurations. In the E-plane, θ_{max} reaches 52° and 41° for the 10% and 20% BW goals, respectively. In the H-plane, the improvement is most pronounced with θ_{max} increase to 40° and 26° for the 10%, 20% BW cases. No scan-blindness effects are observed in both

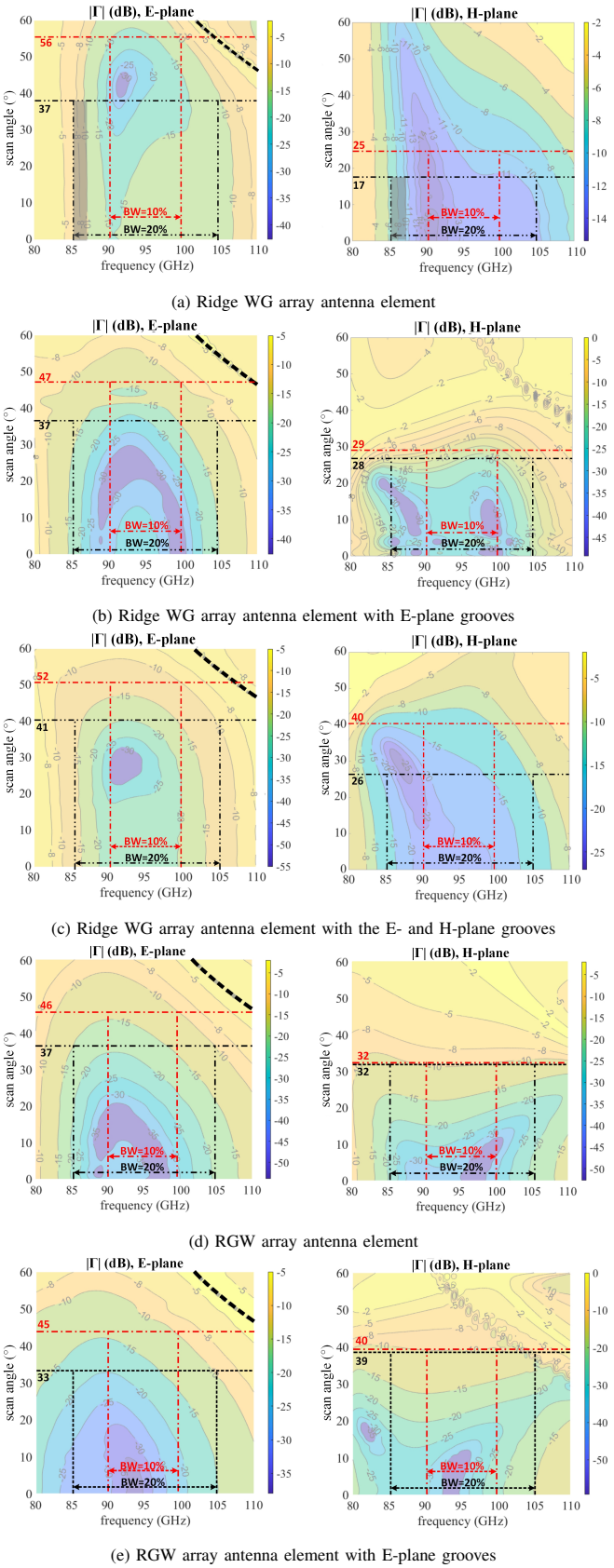

(a) Ridge WG array antenna element

(b) Ridge WG array antenna element with E-plane grooves

(c) Ridge WG array antenna element with the E- and H-plane grooves

(d) RGW array antenna element

(e) RGW array antenna element with E-plane grooves

Fig. 3. Active reflection coefficient (in dB) for various ridge WG and RGW array elements. The black dashed line indicates the grating lobe-free border.

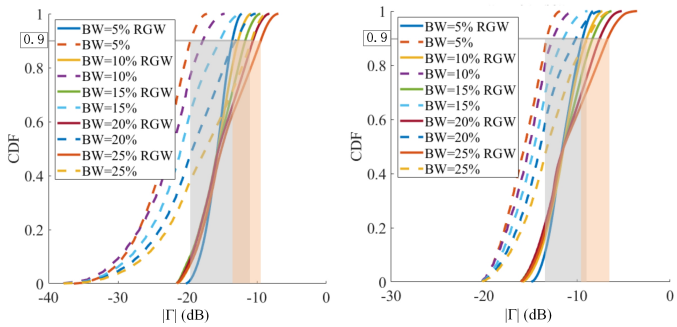

(a) 30–40° scan range, E-plane

(b) 40–50° scan range, E-plane

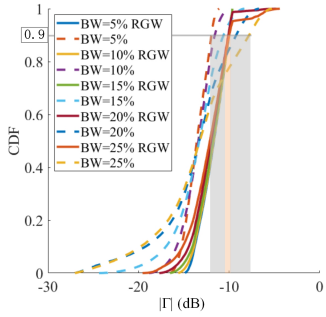

(c) 30–40° scan range, H-plane

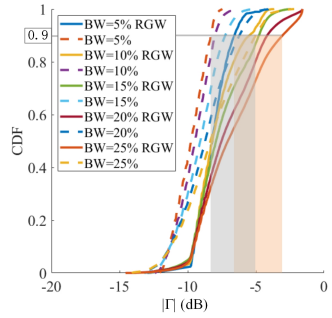

(d) 40–50° scan range, H-plane

Fig. 4. Bandwidth vs. scan range trade-off study results for the following design cases: (i) the RGW antenna element with E-plane grooves (solid lines) and (ii) the ridge WG antenna element with the E- and H-plane grooves (dash lines). CDF is cumulative distribution function.

planes. Compared to the initial ridge WG element design, this design has the largest BW and the widest beam-steering sector.

Finally, Fig. 3(d) shows $|\Gamma|$ of the proposed RGW array antenna element. In this case, θ_{max} is 46° and 37° for the 10% and 20% BW requirements in the E-plane; and 32° for both 10%, 20% BW requirements in the H-plane. The overall performance is better than that of the initial ridge WG element design. However, the scan-blindness exists in both beam-steering planes for large scan angles.

When the pair of E-plane grooves is added, we can observe an unexpected beam-steering performance improvement. Fig.3(e) shows that instead of the expected improvement in the E-plane, the grooves have a major impact on the H-plane beamsteering performance: θ_{max} in the H-plane has been increased to 40° and 39° for the 10% and 20% BW cases. This interesting phenomenon is accompanied by additional H-plane $|\Gamma|$ resonances associated with the scan-blindness. This affects the element's beam-steering performance at $\leq$40° around 105 GHz. The nature of this effect is the same as for the case in Fig. 3(b) (H-plane). We believe that it is related to the surface wave propagation *along* the E-plane grooves and will be explored during future studies.

IV. Bandwidth vs. Scan Range Trade-Offs

In the above analysis, we have defined the operation bandwidth by the $|\Gamma| \leq -10$ dB impedance matching criterion. In practice, this criterion can be relaxed, depending on application. Our results for the proposed RGW design with grooves [see Fig.3(e)] show that the impedance bandwidth starts to shrink when the scan angle reaches 40° in the E-plane, and 30° in the H-plane, which denotes the region of interest for the trade-off analysis. We analyzed $|\Gamma|$ by sweeping the scanning angles in both planes with the bandwidth varying from 5% to 25%. A set of cumulative distribution functions (CDFs) are plotted, as shown in Fig. 4. The CDF is defined as $CDF(x) = P(|\Gamma| \leq x)$, where P denotes the probability function. Simulated results of ridge WG array element with E- and H-plane grooves are introduced here for a more complete comparison.

In the E-plane, both array elements have $\geq$ 90% of $|\Gamma|$ points (CDF $\geq$ 90%) below -10 dB for the 25% BW and 30–40° scan range. When the scan angle increases to 40–50°, the ridge WG array element with the E- and H-plane grooves exhibits better impedance matching with CDF = 90% within 25% BW, as compared to 10% bandwidth of the RGW element. If a $|\Gamma| \leq -7$ dB requirement is acceptable, the bandwidth of the RGW element can be increased to 25%. In the H-plane, the RGW configuration has a wider bandwidth for 30–40° scan range: 90% RGW element's $|\Gamma|$ points fulfill $|\Gamma| \leq -10$ dB reaching 25% BW, and the ridge WG array bandwidth is only 15%. For the scan range of 40–50°, if we select the $|\Gamma| \leq -7$ dB criterion for CDF = 90%, the RGW and WG element designs have 5% and 20% BW, respectively.

In summary, the RGW array element has demonstrated promising beam-steering performance, where up to 25% impedance bandwidth (which is defined for the 90% CDF level for $|\Gamma| \leq -10$ dB) is achieved over the scan range of $\pm$40° in both E- and H-planes. A wider scan range of $\pm$50° is possible for a relaxed criterion of $|\Gamma| \leq -7$ dB. The RGW element with the grooves outperforms the initial ridge WG array element design with the E- and H- plane grooves for the H-plane scanning scenario, though at the cost of the reduced performance in the E-plane. Nonetheless, in overall, the RGW structure has an important advantage of enabling contactless transition to active electronics while being also less prone to manufacturing and assembling errors that are critical at W-band or higher frequencies.

V. Conclusion

We have considered several possible implementations of array antenna elements for future B5G communication systems at W- and D-band frequencies. These designs are based on the open-ended ridge or ridge gap WG elements, which are capable of simultaneously providing wideband and wide-angle array beam-steering performance with high radiation efficiency. The full-wave simulation results reveal two best element configurations, among the considered ones, where we have introduced decoupling grooves in the WG aperture (namely, the ridge WG element with the E- and H-plane grooves and the RGW element with the E-plane grooves). The best RGW element design is capable of realizing $\pm$40° scan range in both E- and H-planes within the 25% bandwidth ($|\Gamma| \leq -10$ dB). This promising beam-steering capability,

along with possible contactless RGW interface towards active electronics, makes this RGW array element a suitable candidate for future 100+GHz electronically scanned array antennas. The experimental study of the proposed antenna concepts is on-going and will be demonstrated through a finite array fragment characterization.

A further improvement of beam-steering performance could be achieved applying more effective elements decoupling techniques, especially in the H-plane. This is a subject of the future research.

ACKNOWLEDGMENT

This work has received funding from the European Union's Horizon 2020 research and innovation programme under the Marie Skłodowska-Curie grant agreement No 860023 (for the contributions by Y. Zhang and A.R. Vilenskiy) and the Sweden-Taiwan Collaborative Research Framework Project "Antenna Technologies for Beyond-5G Wireless Communication" from the Swedish Foundation for Strategic Research's (for the contribution by M. Ivashina).

REFERENCES

[1] Z. W. Miao, Z. C. Hao, G. Q. Luo, L. Gao, J. Wang, X. Wang, and W. Hong, "140 GHz high-gain ltcc-integrated transmit-array antenna using a wideband siw aperture-coupling phase delay structure," *IEEE Trans. Antennas Propag.*, vol. 66, no. 1, pp. 182–190, 2018.

[2] D. Kim, J. Hirokawa, M. Ando, J. Takeuchi, and A. Hirata, "64×64-element and 32×32-element slot array antennas using double-layer hollow-waveguide corporate-feed in the 120 GHz band," *IEEE Trans. Antennas Propag.*, vol. 62, no. 3, pp. 1507–1512, 2014.

[3] S. S. Yao and Y. J. Cheng, "W-band high-efficiency wideband planar array antenna based on mems micromachining technology," in *2018 48th European Microwave Conference (EuMC)*. IEEE, 2018, pp. 942–945.

[4] A. Gomez-Torrent, M. Garcia-Vigueras, L. Le Coq, A. Mahmoud, M. Ettorre, R. Sauleau, and J. Oberhammer, "A low-profile and high-gain frequency beam steering subterahertz antenna enabled by silicon micromachining," *IEEE Trans. Antennas Propag.*, vol. 68, no. 2, pp. 672–682, 2019.

[5] A. B. Numan, J.-F. Frigon, and J.-J. Laurin, "Printed w-band multibeam antenna with luneburg lens-based beamforming network," *IEEE Trans. Antennas Propag.*, vol. 66, no. 10, pp. 5614–5619, 2018.

[6] U. Kodak, B. Rupakula, S. Zihir, and G. M. Rebeiz, "60- GHz 64- and 256-element dual-polarized dual-beam wafer-scale phased-array transceivers with reticle-to-reticle stitching," *IEEE Trans. Microw. Theory Tech.*, 2020.

[7] A. Aljarosha, A. U. Zaman, and R. Maaskant, "A wideband contactless and bondwire-free mmic to waveguide transition," *IEEE Microw. Wireless Compon. Lett.*, vol. 27, no. 5, pp. 437–439, 2017.

[8] M. K. Leino, R. Montoya Moreno, J. Ala-Laurinaho, R. Valkonen, and V. Viikari, "Waveguide-based phased array with integrated element-specific electronics for 28 GHz," *IEEE Access*, vol. 7, pp. 90 045–90 054, 2019.

[9] Y. Rong and K. A. Zaki, "Characteristics of generalized rectangular and circular ridge waveguides," *IEEE Trans. Microw. Theory Tech.*, vol. 48, no. 2, pp. 258–265, 2000.

[10] J. Montgomery, "Ridged waveguide phased array elements," *IEEE Trans. Antennas Propag.*, vol. AP-24, no. 1, pp. 46–53, 1976.

[11] S. Wand and A. Hessel, "Aperture performance of a double-ridge rectangular waveguide in a phased array," *IEEE Trans. Antennas Propag.*, vol. AP-26, no. 2, pp. 204–214, 1978.

[12] A. K. Bhattacharyya, *Phased array antennas: Floquet analysis, synthesis, BFNs and active array systems*. John Wiley & Sons, 2006, vol. 179.

[13] P.-S. Kildal, A. A. Kishk, and S. Maci, "Special issue on artificial magnetic conductors, soft/hard surfaces, and other complex surfaces," *IEEE Trans. Antennas Propag.*, vol. 53, no. 1, pp. 2–7, 2005.

[14] A. U. Zaman and P.-S. Kidal, *Gap Waveguide in Handbook of Antenna Technologies*. New York, NY: Springer Science+ Business Media Singapore, 2015, p. 464.